

RESEARCH ARTICLE

10.1002/2015JC011177

Regulation of South China Sea throughflow by pressure difference

Huiling Qin¹, Rui Xin Huang^{1,2}, Weiqiang Wang¹, and Huijie Xue^{1,3}

Key Points:

- Pressure head existing between the WP and the EIO is correlated with the KSSTF on decadal time scale
- Pressure head between the WP and the Sulawesi Sea corresponds to the MSTF on interannual time scale
- SSH difference is decomposed into the integrated thermal and haline terms with the thermal contribution accounting for ~ 58% for the KSSTF but close to 90% for the MSTF

Correspondence to:

W. Wang,
weiqiang.wang@scsio.ac.cn

Citation:

Qin, H., R. X. Huang, W. Wang, and H. Xue (2016), Regulation of South China Sea throughflow by pressure difference, *J. Geophys. Res. Oceans*, 121, 4077–4096, doi:10.1002/2015JC011177.

Received 28 JUL 2015

Accepted 17 MAY 2016

Accepted article online 19 MAY 2016

Published online 12 JUN 2016

¹State Key Laboratory of Tropical Oceanography, South China Sea Institute of Oceanology (SCSIO), Chinese Academy of Science, Guangzhou, China, ²Department of Physical Oceanography, Woods Hole Oceanographic Institution, Woods Hole, Massachusetts, USA, ³School of Marine Sciences, University of Maine, Orono, Maine, USA

Abstract Sea Surface Height (SSH) data from the European Centre for Medium-Range Weather Forecasts–Ocean Reanalysis System 4 (ECMWF-ORAS4) are used to determine the pressure difference in connection with variability of the South China Sea ThroughFlow (SCSTF) from 1958 to 2007. Two branches of SCSTF, the Karimata-Sunda Strait ThroughFlow (KSSTF) and the Mindoro Strait ThroughFlow (MSTF), are examined. Using the ensemble empirical mode decomposition method (EEMD), time series of pressure difference and volume transport are decomposed into intrinsic mode functions and trend functions, with the corresponding variability on different time scales. Pressure difference agrees with the KSSTF volume transport on decadal time scale; while for the MSTF, pressure difference varies similarly with volume transport on interannual time scale. Separating the dynamic height difference into the thermal and haline terms, for the KSSTF more than half of the dynamic height difference (32 cm) is due to the thermal contributions; while the remaining dynamic height difference (23 cm) is due to the haline contributions. For the MSTF, the dynamic height difference (29 cm) is primarily due to the thermal contribution (26 cm).

1. Introduction

The South China Sea Throughflow (SCSTF) is a loosely defined term describing the collection of currents from the Western Pacific (WP) to the Eastern Indian Ocean (EIO) through the South China Sea (SCS), including the inflow through the Luzon Strait and the outflows through the Karimata-Sunda and Mindoro Straits. Its existence has been discussed in many previous publications. For example, *Qu et al.* [2005] pointed out its existence in a model simulation; *Yu et al.* [2007] revealed the existence of the SCSTF from satellite images and numerical experiments; *Yaremchuk et al.* [2009] also inferred it from climatological temperature and salinity data of World Ocean Atlas 2001.

The SCSTF is a critical component linking large-scale circulations in the Pacific and Indian oceans [*Qu et al.*, 2006]. It is also part of the circulation system in the SCS. It transports Kuroshio water into the SCS, carrying the large-scale climate signals in the WP into the SCS. In terms of water mass, heat, and freshwater balance, around 10 percent of the Kuroshio is transported into the SCS through the Luzon Strait. It represents a nonnegligible reduction in the Kuroshio's poleward transport of water mass, heat, and freshwater [*Yu et al.* 2007]. On the other hand, water exiting the SCS through the Mindoro Strait and Karimata-Sunda Strait plays an active role in transporting water mass, heat, and freshwater from the WP to the Indian Ocean [*Qu et al.* 2006; *Yu et al.* 2007].

Recently, the variability of SCSTF on seasonal to decadal time scales has been studied intensively, e.g., *Liu et al.* [2012], *Wang et al.* [2006], and *Yu and Qu* [2013]. Most of these studies are focused on the role of wind stress anomaly as the main driver for SCSTF variations, using the "island rule" or numerical model output. However, our study is focused on the pressure difference between the beginning and end of the throughflow.

The oceanic general circulation can be conceptually separated into the wind-driven circulation (WDC) and thermohaline circulation (THC). The WDC is primarily confined to the upper kilometer of the ocean, but the THC exists over the entire depth of the ocean. We argue that the pressure difference along the pathway of the throughflow is set up by both the THC and the WDC, and we postulate that this pressure difference can be used as an index for the SCSTF. Up until now, the role of pressure difference in regulating SCSTF has not received adequate attention because of the complicated topography and intricate ocean circulations in the SCS; thus, we will examine some of the relevant physics in detail.

Large-scale motions in the interior of a stratified ocean, away from the bottom/lateral boundaries, are nearly geostrophic. By definition, geostrophic currents flow mostly along pressure contours; the pressure field itself is in turn set up by the basin-scale WDC and THC. However, currents through relatively narrow channels/passages are directly linked to the along-stream pressure difference that counter balances the friction along the lateral/bottom boundaries. In the open ocean, such pressure difference can be easily identified from the sea surface height (SSH) difference.

Many researches have confirmed the dynamic connection between flows through a narrow strait and sea level pressure difference upstream and downstream of the strait, such as the flow through the Bering Strait [Aagaard *et al.* 1985; Overland and Roach, 1987; Roach *et al.*, 1995], Tsushima Strait [Takikawa and Yoon, 2005; Morimoto and Yanagi, 2001], Indonesia Throughflow (ITF) [Wyrki, 1987; Tillingner and Gordon, 2009], and the Luzon Strait [Xue *et al.*, 2004; Nan *et al.*, 2013]. The flow through the Bering Strait is a good example. Although the local wind tends to blow southward, a sea level gradient associated with the large-scale circulation in the northern North Pacific and Arctic Ocean drives a northward mean flow from the Pacific Ocean to the Chukchi Sea through the Bering Strait, as discussed in Overland and Roach [1987].

Although the pioneering work of Wyrki [1961, 1987] was mostly focused on the role of wind stress, the contribution from thermohaline circulation in regulating ITF is nonnegligible, as discussed in many papers published afterward, e.g., Gordon and Fine [1996]. Therefore, we postulate that the pressure difference between the WP and the EIO regulates the SCSTF, which is regarded as a part of the ITF, in particular on interannual and decadal time scales. Similar to the ITF, the pressure difference regulating the SCSTF is set up by the WDC and the THC as follows.

1. In the WP, the prevailing trade winds over the tropical ocean and the anticyclonic wind-driven gyre generate a high sea level near the western boundary, while in the EIO trade winds in the tropical Southern Hemisphere pull water away from the eastern boundary. Because the Indonesian waters are located upstream to the EIO, the corresponding sea level is also relatively low, i.e., there is a SSH difference between the WP and the Indonesian waters induced by wind stress forcing.
2. As described by Talley *et al.* [2011], precipitation overpowers evaporation in the Pacific Ocean; thus, water in the Pacific basin is fresher than in the IO. The differences in temperature and salinity profiles in the WP and the EIO result in density profile difference, which in turn enhances the SSH difference induced by wind stress.

Exploring physical processes controlling regional SSH changes is important for our understanding of the connection between pressure difference and the SCSTF variations. Cazenave and Lovel [2010] pointed out that steric changes arising from ocean density variations are the main cause of low-frequency sea level variability in most regions. Here, the term “steric change” is strictly regarded as the change induced by temperature, salinity, and pressure-dependent-specific volume of the ocean. Similar to their method, dynamic height changes can be interpreted in terms of density changes associated with temperature and salinity variations.

Large-scale circulation changes, on the other hand, may redistribute characteristic water masses and, thus, lead to different dynamic height changes regionally. The diagnosis of dynamic height changes, through decomposition of thermal and haline contributions, can help us to understand the physical processes regulating SSH variability induced by changes in basin-scale WDC and THC. However, stratification in the ocean is the result of the nonlinear interaction of WDC and THC. As such, the partition of SSH variability due to WDC and THC cannot be separated completely; thus, this is not discussed in the present study.

This paper is organized as follows: section 2 introduces the data and methods used in this study. Section 3 shows the relationship between the SCSTF and variation of pressure-head between WP and EIO. In section 4, SSH changes due to temperature and salinity anomalies at each depth are analyzed. Finally, we draw the conclusions in section 5.

2. Data and Method Introduction

2.1. Ocean Reanalysis Data

In this study, we use reanalysis data from two models: the European Centre for Medium-Range Weather Forecasts-Ocean Reanalysis System 4 (ECMWF-ORAS4, ORAS4 hereafter) and Simple Ocean Data Assimilation (SODA) reanalysis. The 50 year reanalysis data (1958–2007) used in this study includes monthly mean

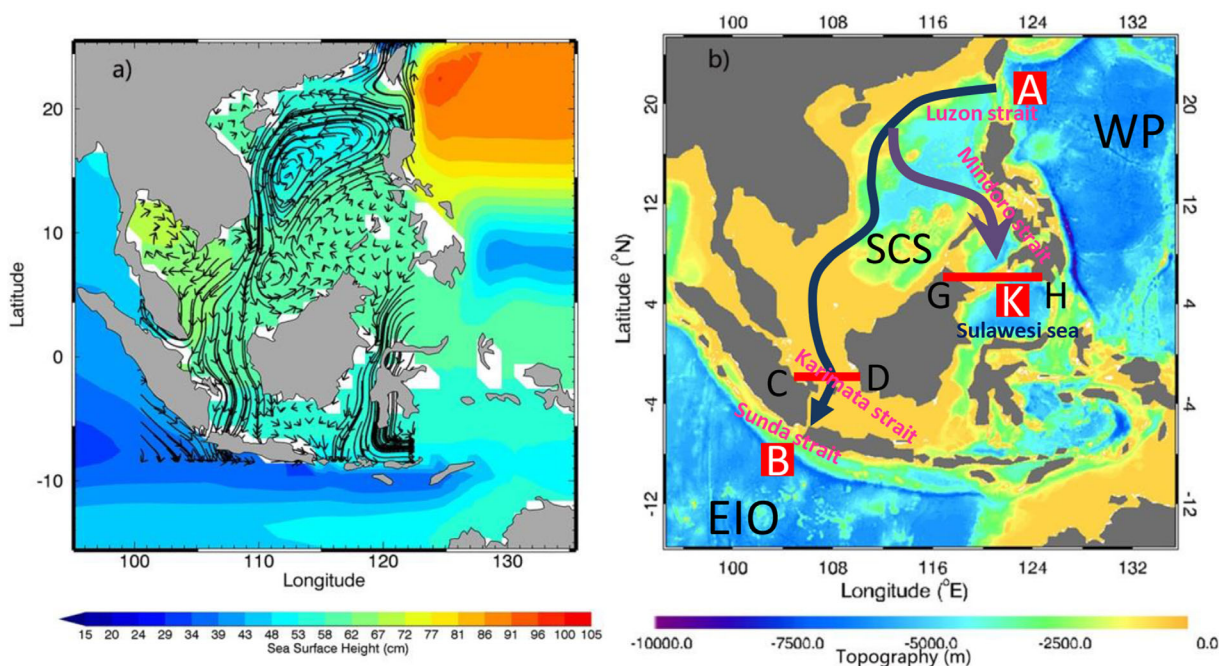


Figure 1. (a) SSH and streamlines of ocean currents in top 50 m layer in the SCS from ORAS4, averaged over 1958–2007. (b) Topography of the SCS and the sketch of two branches of SCSTF based on streamlines in Figure 1a. For the KSSTF branch, Kuroshio water enters the northern SCS via the Luzon Strait, and exits from the Karimata-Sunda Strait, feeding the EIO. For the MSTF branch, water exits from the Mindoro Strait, then feeding the Sulawesi Sea. Region A is located at (18.5°–21.5°N, 123.5°–125.5°E), while region B is located at (7.5°S–10.5°S, 103.5°–106.5°E). Region K is located at (2.5°–4.5°N, 121.5°–124.5°E); CD is located at (2.5°S, 104.5°–110.5°E); GH is located at (6.5°N, 117.5°–124.5°E).

velocity, wind stress, temperature, salinity, and sea level data. They are used in the calculation of sea level pressure difference, including the contributions from temperature and salinity. ORAS4 is forced by daily surface fluxes of solar radiation, total heat flux, evaporation-minus-precipitation, and surface wind stress. They are taken from the ECMWF Re-Analysis (ERA) 40 from September 1957 to December 1989, and from ERA-Interim from January 1989 to December 2009. The assimilated observations include the historical archive of hydrographic profiles by ships, moored hydrographic observations, altimetry, and Argo data. The horizontal resolution of ORAS4 is $1.0^\circ \times 1.0^\circ$. There are 42 nonuniform vertical levels (22 levels in the upper 500 m). Details of the ORAS4 data set used in this analysis can be found in *Balmaseda et al.* [2013].

The Simple Ocean Data Assimilation (SODA) products, version 2.0.2 for 1958–2001 and 2.0.4 for 2002–2007, are used in this study for a comparison with ORAS4. SODA_2.0.2 is forced by daily wind stress and heat flux from the ERA-40 atmospheric reanalysis, while SODA_2.0.4 is forced by QuikSCAT winds. Surface freshwater flux is provided by the Global Precipitation Climatology Project (GPCP) monthly satellite-gauge merged product combined with evaporation from bulk formula, for the period from January 1979 to December 2007. The assimilated observations include the historical archive of hydrographic profiles by ships, moored hydrographic observations, and remotely sensed Sea Surface Temperature (SST). The horizontal resolution of SODA is $0.5^\circ \times 0.5^\circ$, and there is a total of 40 vertical levels with 19 levels in the upper 500 m. Details of the SODA data set used in this analysis can be found in *Carton and Giese* [2008]. *D'Addezio et al.* [2015] conducted a specific comparison of the two reanalysis data sets. They suggested that although ORAS4 and SODA (version: SODA_2.2.4) both assimilate *in situ* data like hydrographic profiles by ships, moored hydrographic observations, etc., the data sources are not identical and quality-controlled procedures are different, which can lead to differences between them. Different model resolutions may be another reason for differences between ORAS4 and SODA.

We first examine the climatological mean of ORAS4 to illustrate the suitability of ORAS4 in SCSTF studies. Figure 1a shows the mean SSH and streamlines of ocean currents in the upper 50 m of the SCS averaged over 1958–2007 from the ORAS4. The SSH decreases from the WP, the SCS to the EIO. The streamlines in the upper 50m indicate the flow through the Karimata-Sunda Strait and the flow through the Mindoro Strait, i.e., the exits of both branches of the SCSTF. Figure 1b shows the topography of the SCS and a sketch of two branches of the SCSTF (thick curves). The first branch is called the Karimata Sunda Strait/Shelf

Throughflow (KSSTF) in this study, which consists of Kuroshio water entering the northern SCS via the Luzon Strait and exiting from the Karimata Strait, and finally feeding into the EIO via the Sunda Strait. *Qu et al.* [2006] suggested that mass flux through the Karimata Strait is further separated into three branches: Celebes Sea, Flores Sea, and the Lombok Strait. They did not mention the transport through the Sunda Strait. However, in the ORAS4 simulation, transport through the Sunda Strait consists of a major portion (70%) of this throughflow branch; thus, we name this branch tentatively as the KSSTF in this study. The second branch is called the Mindoro Strait Throughflow (MSTF), which consists of water exiting through a 420 m deep channel of the Mindoro Strait, and then feeding into the Sulawesi Sea. Figure 1a also clearly shows the large SSH differences between the beginnings and ends of these two oceanic pathways discussed above (the red squares A and K in Figure 1b).

Xu and Oey [2014] listed several *in situ* observations of Luzon Strait (LS) volume transport together with their model simulation results. We compare LS volume transports of ORAS4 with the values in *Xu and Oey* [2014]: the long-term annual mean transports are comparable. However, the volume transport of ORAS4 is larger than *Xu and Oey* [2014] in the upper layer, and it is smaller in middle and low layers. Since our study is focused on the variability of whole LS transport, the differences in the partition of transport between layers do not affect our conclusions. We also compare monthly values obtained from ORAS4 with *in situ* observations [see *Xu and Oey*, 2014, Table 3]. In March 1992, the ORAS4 LS transport values are quite close to the results reported by *Yuan et al.* [2009]. In ORAS4, it is -7.6 Sv in the upper 0–500m, while *Yuan et al.* [2009] observed -6.6 Sv in the upper 0–400m. In the bottom layer (1500–bottom), ORAS4 has 0.5 Sv inflow, while *Yuan et al.* [2009] observed 0.1 Sv inflow. In August and September 1994, ORAS4 has 0.29 Sv outflow in the middle layer, which is very close to the 0.22 Sv reported by *Yuan et al.* [2008]. *Gordon et al.* [1999] reported the Makassar volume transport from late 1996 to June 1998. We compare Makassar volume transport of ORAS4 (2.5S, 116.5–119.5°E, figure not included) with *in situ* observations [*Gordon et al.*, 1999, Figures 3 and 4]. The corresponding annual mean value is quite close to that recorded in 1997. ORAS4 has a 10.3 Sv southward flow, while *Gordon et al.* [1999] observed a value of 9.3 Sv. The annual cycle is also consistent with a maximum in June and a minimum in December. *Gordon et al.* [1999] pointed out: “A strong intra-seasonal event occurs from late May to July 1997.” ORAS4 simulation also indicates an intraseasonal event in this period, but with weaker magnitude.

On the other hand, some of the narrow straits in Indonesian waters are not properly resolved in ORAS4 at the $1.0^\circ \times 1.0^\circ$ horizontal resolution. For example, although the sill depth of the Sunda Strait (~ 100 m) is accurately represented in the model, this strait is artificially widened and represented by one interior grid in terms of the velocity in ORAS4 (hence the effective width is about 110 km). This is a rather crude representation of the Sunda Strait for its actual width is only 24 km based on ETOPO2, the Global 2 Arc-minute Ocean Depth and Land Elevation data. As a result, most of the transport of the KSSTF flows to the EIO through this strait (0.55 Sv for the 50 year mean from 1958 to 2007) in ORAS4 with very little going through the eastern Java Sea to exit the Lombok Strait (~ 0.14 Sv for the 50 year mean). On the other hand, the *in situ* observations indicate that only a small portion of the KSSTF goes to the EIO through the Sunda Strait [*Fang et al.*, 2005; *Susanto et al.*, 2013] while the majority takes the Lombok Strait [*Gordon et al.*, 2010]. The latter is also in agreement with the analysis of *Qu et al.* [2005] and the model result of *Castruccio et al.* [2013]. Despite the miss represented exit of the KSSTF arisen most likely from the resolution caused distortion of the straits in ORAS4 hence the large difference between the ORAS4 simulated and the observed volume flux through the Sunda Strait and the Lombok Strait, the SSH immediately outside the exit, also extracted from ORAS4, should be dynamically consistent with the outflow through the corresponding strait. As such the section CD and region B outside of the Sunda Strait (Figure 1b) are chosen in this study to diagnose the mechanism responsible for regulating the KSSTF volume flux partition and the corresponding variability.

Similar analysis using SODA data is also carried out (see Appendix A). Because the 50 year mean, upper layer MSTF is reversed in direction, ORAS4 is selected as the primary data set in this study. Note that both ORAS4 and SODA are data assimilative products. As such, mass, heat and energy of the model are not necessarily conserved.

2.2. Pacific Decadal Oscillation (PDO) Index and Nino 3.4 Index

In order to find the possible causes of pressure difference variation, we use the Pacific Decadal Oscillation (PDO) index and Nino 3.4 index obtained from the website of Earth System Research Laboratory, National Oceanic and Atmospheric Administration (NOAA) (<http://www.esrl.noaa.gov/psd/data/climateindices/list/>).

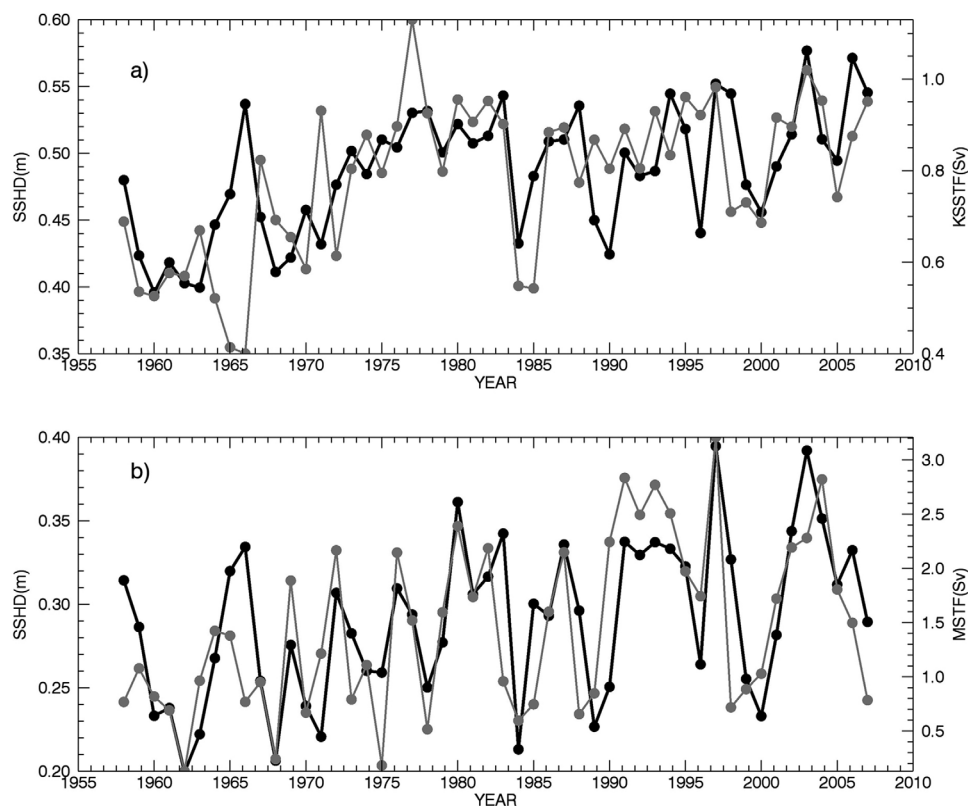


Figure 2. The annual mean time series of (a) SSH difference between region A and B (black) and volume transport (gray) through section CD; (b) SSH difference between region A and K (black) and volume transport (gray) through section GH.

The PDO index is derived as the leading principal component of the monthly SST anomalies in the North Pacific Ocean, poleward of 20°N [Mantua *et al.*, 1997]. The Nino 3.4 index is the monthly SST anomalies in the eastern central tropical Pacific region of ($170^{\circ}\text{--}120^{\circ}\text{W}$, $5^{\circ}\text{N--}5^{\circ}\text{S}$).

2.3. EEMD Analysis

Empirical mode decomposition (EMD) is a method that decomposes a time series into a finite number of intrinsic mode functions (IMFs) and a “monotonous” trend function [Huang *et al.*, 1998]. The number of extrema and the number of zero crossings in each IMF must either equal or differ at most by one. The mean of each IMF is zero. Compared with Fourier and wavelet analysis, EMD has its advantage because of its adaptive basis, while Fourier and wavelet analyses assume predetermined base functions for decomposition. EMD is applicable to nonlinear and nonstationary processes. This study used the ensemble empirical mode decomposition (EEMD) [Wu and Huang, 2009] to acquire significant IMFs. EEMD is a noise-assisted data analysis method, and its application is as follows: (1) adding a white noise series to the targeted data, and then decomposing the data into IMFs; (2) repeating this process again and again with a different white noise series each time; (3) obtaining the mean of corresponding IMFs from a specified number of realizations. It requires two input parameters: the number of ensemble realizations and the amplitude of added white noise. We utilize 800 ensemble realizations with the noise amplitude being 20% of the standard deviation of the original time series. An IMF, which exceeds the 95% confidence level, is statistically significant. The code is provided by Research Center for Adaptive Data Analysis, Taiwan (<http://rcada.ncu.edu.tw/research1.htm>). Readers may refer to Wu and Huang [2009] for the details. Some typical examples of applying EEMD to geophysics data can be found in Palacz *et al.*, [2011], Qian *et al.* [2011], and Franzke [2012].

3. The Relationship Between SCSTF and Pressure-Head

For the KSSTF, the mean SSH difference between east of the Luzon Strait and south of the Sunda Strait is approximately 40–50 cm (Figure 1a). Forced by such a large pressure difference, water enters the SCS

Table 1. Dominant Periods Associated With IMFs of Pressure Difference and Volume Transport of the KSSTF and MSTF, Based on Power Spectrum Analysis, in Unit of Year^a

IMF No.	KSSTF			MSTF		
	Pressure Difference	Volume Transport	Correlation Coefficients	Pressure Difference	Volume Transport	Correlation Coefficients
1	0.50	1.00	-0.07	0.5	0.50	0.03
2	1.00	1.00	-0.37	1.00	1.00	0.08
3	1.00	2.38	-0.06	2.08	1.85	0.29
4	2.77	5.00	0.07	5.57	3.57	0.43
5	5.00	7.16	0.06	8.30	5.55	0.65
6	16.00	16.60	0.45	16.60	12.50	0.60
7	33.00	33.00	0.82	33.00	25.00	0.36

^aThe correlation coefficients of each IMF pair of pressure difference and volume transport are also listed. Values in italics indicate the IMF pairs that do not pass the significance test.

through the Luzon Strait (around 3.8 Sv, 1 Sv $\equiv 10^6 \text{ m}^3 \text{ s}^{-1}$) [Qu *et al.*, 2006]. After complicated routes, it exits through the Karimata Strait (around 1.7 Sv; note that this area is called Sunda shelf in Qu *et al.* [2004]) as schematically shown in Figure 1b. Through field observations, Susanto *et al.* [2013] revealed that the SCSTF via the Karimata Strait appears in the form of “a stronger southward flow in boreal winter and weaker southward bottom flow in boreal summer, beneath the upper layer northward (reversal) flow.” The existence of year-around southward flow is consistent with the north-south SSH slope shown in Figure 1a. In other words, although the local wind stress may affect the Karimata transport, especially within the surface part of the strait, the vertically integrated transport through the Karimata Strait is regulated primarily by the pressure difference/SSH slope set up by large-scale WDC and THC, as discussed above.

For the MSTF, there is also a large SSH difference between east of the Luzon Strait and the Sulawesi Sea. The climatological mean SSH difference is approximately 30 cm. Forced by this pressure difference, water enters the SCS through the Luzon Strait and exits through the Mindoro, as shown in Figure 1. Fang *et al.* [2005] pointed out that water flows out of the SCS through the Mindoro Strait year-round and the corresponding flux is about 1.77 Sv, while Qu and Song [2009] reported the flux of 2.4 Sv.

On the WP side, in the beginning of the SCSTF, region A (18.5–21.5°N, 123.5–125.5°E) is selected to represent regional characteristics east of the Luzon Strait. Since the deep water overflow through the Luzon Strait may induce motions near the 2000 db reference level, region A is located slightly east of the Luzon Strait. Similarly, to avoid the influence of outflow through the Sunda Strait, region B on the EIO side is located at (7.5°S–10.5°S, 103.5–106.5°E), slightly away from the Sunda Strait. The time series of SSH difference between regions A and B is used as an index for monitoring the pressure-head between the WP and EIO. The transport through the Karimata Strait (positive southward) is calculated by vertically and zonally integrating the meridional flow passing through the CD section (2.5°S, 104.5–110.5°E). Mean wind stress (from SODA data) over the CD section is also calculated to represent the local wind stress effect on the KSSTF.

The MSTF shares the same upstream location A with the KSSTF. The end of this pathway (region K in the Sulawesi Sea) is located at (2.5–4.5°N, 121.5–124.5°E). The transport of the MSTF (positive southward) is calculated by vertically and zonally integrating the meridional flow passing through the GH section (6.5°N, 117.5–124.5°E) and the local wind stress in the Mindoro Strait is calculated over this GH section as well.

Table 2. Dominant Period (year) and Variances (m^2) of IMFs of SSH in Region A, B, and K

IMF No.	Region A		Region B		Region K	
	Dominant Period	Variance(x1E-4)	Dominant Period	Variance(x1E-4)	Dominant Period	Variance(x1E-4)
1	0.41	4.26	0.50	2.03	0.50	0.55
2	1.00	16.24	1.00	5.25	1.00	2.05
3	2.50	2.13	1.52	2.56	2.50	2.87
4	5.55	3.83	3.85	2.14	3.57	3.71
5	7.14	1.78	5.00	0.60	5.55	2.41
6	25.00	0.82	16.51	0.76	16.50	1.54
7	33.00	0.57	33.00	0.24	33.00	1.14
Trend		10.50		2.87		2.87

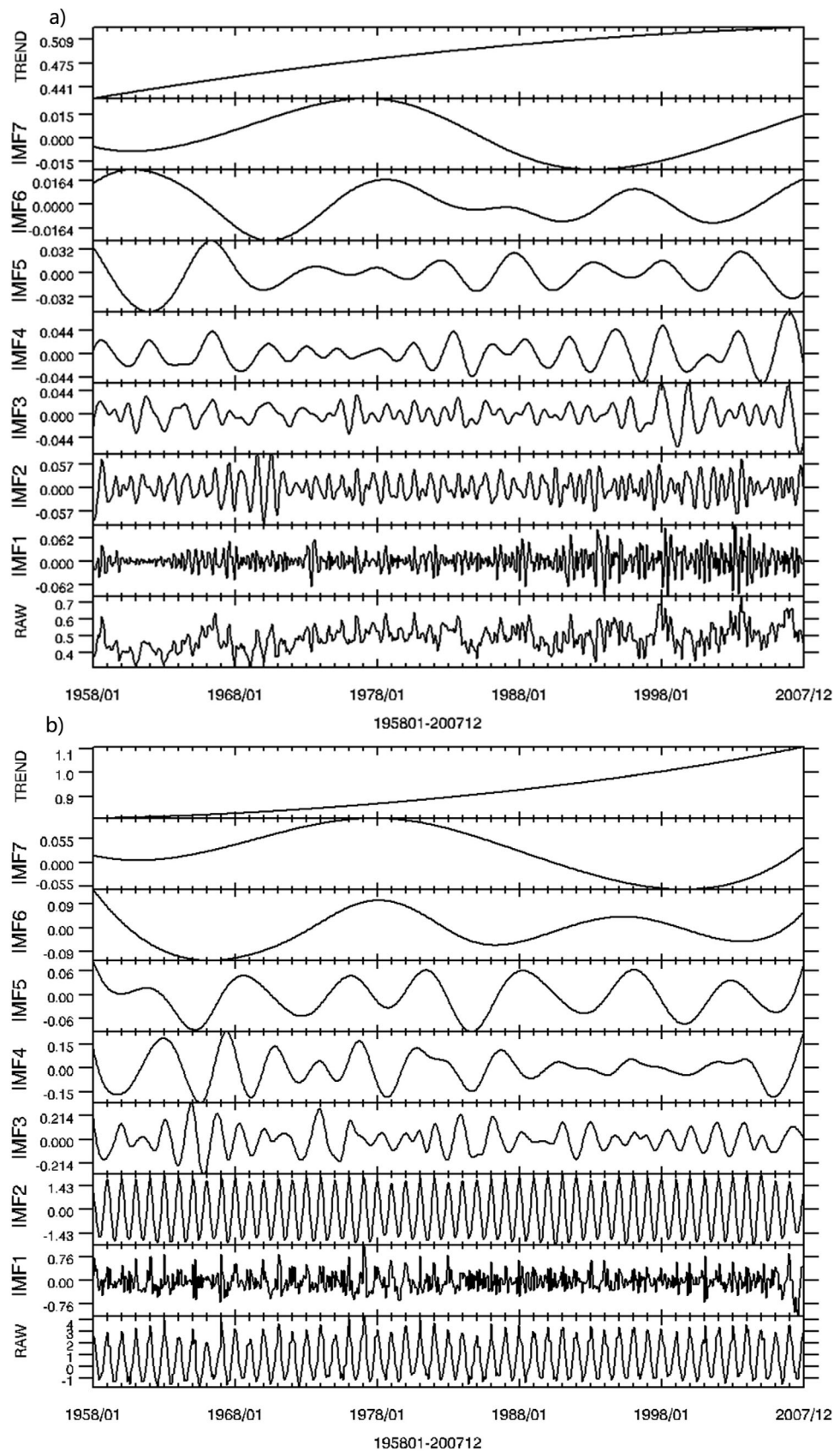


Figure 3. (a) Time series of pressure difference data, defined as the SSH averaged over region A (18.5–21.5°N, 123.5–125.5°E) minus the SSH averaged over region B (7.5°S–10.5°S, 103.5–106.5°E), and the corresponding EEMD components (seven intrinsic mode functions and one trend function), in unit of m. (b) Time series of zonal volume transport through section CD (2.5°S, 104.5°E–110.5°E), in unit of Sv.

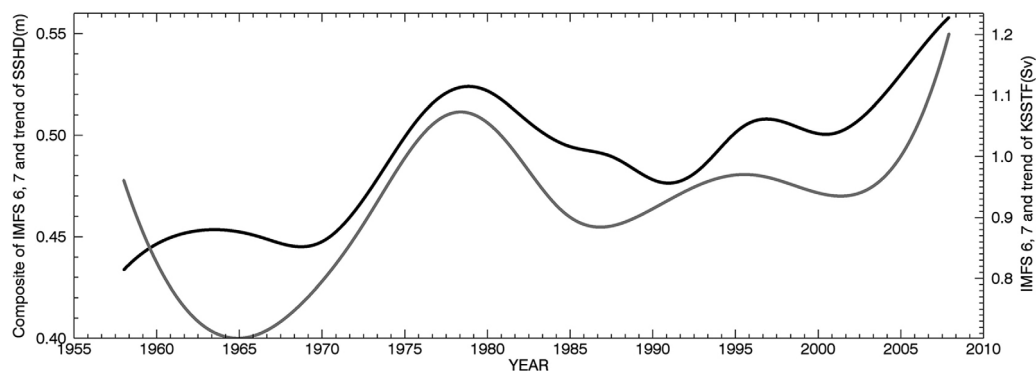


Figure 4. Time series of the combination of the sixth, seventh intrinsic mode functions, and trend function of the EEMD of pressure head (black) and the combination of the sixth, seventh intrinsic mode function, and trend function of volume transport of the KSSTF (gray) in Figure 3.

Figure 2 shows time series of the annual mean pressure difference (gray) and volume transport (black), for the KSSTF (top plot) and the MSTF (bottom plot). In the top plot, the mean sea surface height difference is 49 cm, and the mean KSSTF is 0.79 Sv. Time series show a consistent and significant decadal trend, decreasing before 1965~1970 and increasing afterward. However, on the interannual time scale, the pressure difference and volume transport are not always correlated to each other. The correlation coefficient between the SSH difference and the volume transport is 0.54 with a p -value less than 0.01. Since wind stress is not available as part of the ORAS4, we use SODA wind stress data. The correlation between the volume transport and SODA zonal/meridional wind stress is $-0.06/0.05$. Apparently, in the Sunda shelf, wind stress is not an important term for the vertically integrated momentum balance in the along-channel direction.

In the bottom plot (Figure 2b), the mean SSH difference is 29 cm, and the mean MSTF transport is 1.45 Sv (Figure 2b). The long-term trend is smaller, compared to that of the KSSTF. However, the interannual variations are remarkably consistent between the pressure difference and the volume transport for the MSTF. The correlation coefficient between SSH difference and volume transport is 0.69 with a p -value less than 0.01. However, it is 0.14/0.18 between volume transport and zonal/meridional wind stress over section GH. The correlation between wind and MTSF is poor because water in section GH is deep, as shown in Figure 1b.

In order to identify the SCSTF regulation by pressure difference on different time scales, the EEMD method is used to decompose the monthly mean time series into a finite number of intrinsic mode functions (IMFs), plus a residual "monotonic" trend. For the KSSTF, there are seven IMFs decomposed from the pressure difference and volume transport time series, as shown in Figure 3. Among them, No. 3 and 5 IMFs of volume transport do not pass the significant test, and they are excluded from the interannual or decadal composite below. The dominant period of each IMF defined by spectrum analysis is listed in Table 1.

As shown in Table 1, the first and second IMFs represent the semiannual and annual variations, while the third, fourth, and fifth IMFs correspond to interannual variations. Finally, the sixth and seventh IMFs indicate decadal to multidecadal variations. Table 1 also lists the correlation coefficients of each IMF pair of pressure difference and volume transport, for example, the third IMF of pressure difference and third IMF of volume transport being one pair. It can be seen that the No. 6 IMF pair has good correlation compared with other IMF pairs; thus, there is good correlation on decadal to multidecadal time scales.

To demonstrate this relation, we show a composition of sixth, seventh IMFs and trend component of pressure difference and a composition of sixth, seventh IMFs and trend component of KSSTF volume transport in Figure 4. Both pressure difference and volume transport increased from the late 1960s to late 1970s and from late 1992 to 1996. They decreased from 1980 to 1986 and from 1996 to 2001. Thus, on decadal to multidecadal time scales, the KSSTF is regulated by the pressure difference between WP and EIO.

Since pressure difference is defined as the SSH at region A subtracting SSH at region B, the region with the larger variance is the dominant player in regulating the corresponding throughflow. The variances of IMFs of SSH in regions A and B are shown in Table 2.

In general, the variance associated with the annual variability is the largest. However, our interest is focused on decadal time scale, for which the variances of IMFs 6 and 7 are smaller compared to other time scales.

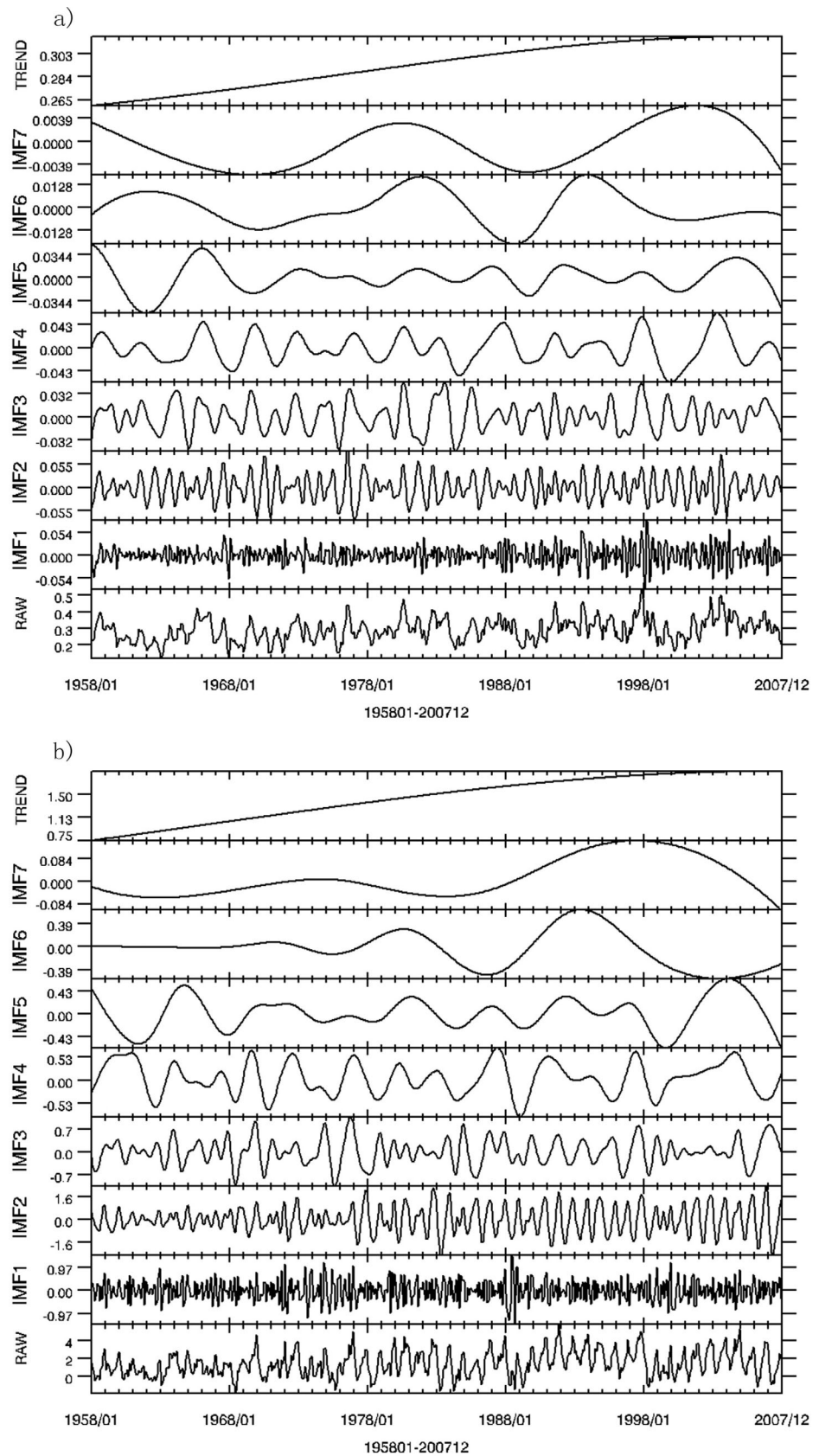


Figure 5. (a) Time series of pressure difference data, defined as the SSH averaged over region A (18.5–21.5°N, 123.5–125.5°E) minus the SSH averaged over region K (2.5–4.5°N, 121.5–124.5°E), and its EEMD components (seven intrinsic mode functions and one trend function), in unit of m. (b) Time series of zonal volume transport through section GH (6.5°N, 117.5–124.5°E), in unit of Sv.

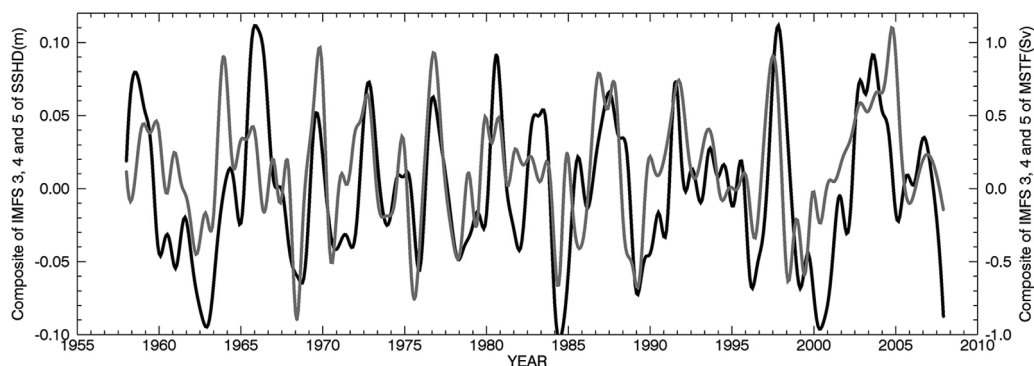


Figure 6. The combined time series (consisting of the third, fourth, and fifth intrinsic mode functions of EEMD components) of pressure head (black) and volume transport (gray) in Figure 5.

For the seventh IMF, the variance of SSH in region A is much larger than that in region B. Hence, on multidecadal time scale (the dominant period is 33 years), the oscillation in pressure difference related to the KSSTF is primarily controlled by SSH variability in region A of the WP, rather than the one in the EIO.

For the sixth IMF, SSH in region A has a dominant period of 25 years, while that in region B is dominated by the signal of 16.6 year periods, which is the same as the dominant period of the sixth IMFs of pressure difference and volume transport shown in Table 1. This indicates that the dominant period of sixth IMF of pressure difference between region A and B is mainly controlled by dynamics in region B. For the trend component, the increasing tendency of pressure difference (around 9 cm from 1958 to 2007, Figure 3a) consists of the increase of SSH in region A, around 11 cm (figures not included) and the increase of SSH in region B, around 2 cm. The increase of SSH in the WP is obviously larger than the increase in the EIO. Such long-term trends and magnitudes of changes in the WP and EIO are consistent with satellite altimetry and tide gauge observations from *Zhang and Church [2012]* and *Han et al. [2014]*.

Using EEMD to analyze the MSTF, we obtain seven IMFs from pressure difference and volume transport time series, as shown in Figure 5. There are the monotonous increasing trends in both pressure difference and volume transport. The dominant periods of IMFs are shown in Table 1. The correlation coefficients of each IMF pair and volume transport show that the third, fourth, fifth, and sixth IMF pairs have good correlation compared to other IMF pairs, as shown in Figure 5. In order to clarify the interannual variability, the combination of the third, fourth, and fifth IMFs is shown in Figure 6. It is clear that the pressure difference and volume transport of the MSTF indicate a good relationship on interannual time scales with correlation coefficient of 0.61. The total variance of the third, fourth, and fifth IMFs of SSH in region K ($8.99 \times 10^{-4} \text{ m}^2$) is larger than that in region A ($7.74 \times 10^{-4} \text{ m}^2$). We can conclude that the SSH in region K contributes more to the pressure difference variability that regulates the MSTF on the interannual time scale. However, in the trend component, the SSH trend in region K is small, less than 5.5 cm (figure not included). Therefore, the increasing trend of pressure difference between regions A and K, around 5.6 cm, is mostly due to the increase of SSH in region A shown in the topmost plot of Figure 5a.

In order to confirm the KSSTF and MSTF variability found in ORAS4, we also use SODA data as verification. SODA covers the same period as ORAS4; however, its horizontal resolution is 0.5 degree, twice the resolution of ORAS4. Figure 7 shows the time series of volume transports from ORAS4 and SODA. They are quite consistent in both the monthly and the annual mean time series. For the KSSTF, the magnitude of ORAS4 is larger than that of SODA by about 0.1 Sv, while for the MSTF, the magnitude of ORAS4 is larger than that of SODA by about 0.9 Sv. The correlation coefficient between SODA and ORAS4 is 0.67 (0.81) for 50 years of the annual mean KSSTF (MSTF). Correlations are significant at the 99% confidence level. Therefore, we consider the variabilities of the KSSTF and MSTF to be robust and consistent in ORAS4 and SODA.

4. The Relationship Between Regional SSH and PDO, ENSO

Among dynamical phenomena, the PDO and ENSO are known to have the largest impact on the decadal and interannual variability of the global climate [*Mantua et al., 1997; Krishnan and Sugi, 2003*]. As discussed

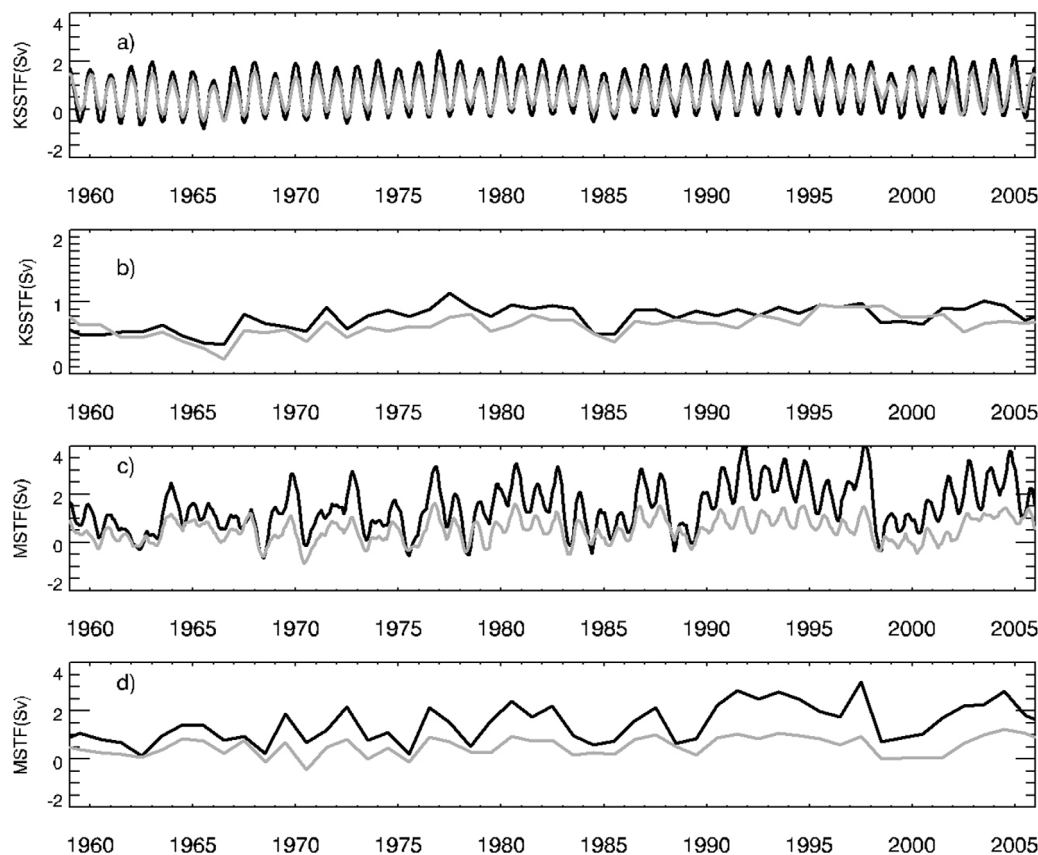


Figure 7. Time series of the volume transport of (a) the monthly mean KSTF, (b) the annual mean KSTF, (c) the monthly mean MSTF, and (d) the annual mean MSTF of different ocean reanalysis data sets which include SODA (gray) and ORAS4 (black). The monthly mean time series have been filtered by 6-point smoothing.

above, the fluctuation of pressure difference is a consequence of regional SSH variation in different ocean basins, and such variability may be closely linked to PDO and ENSO [Frankcombe *et al.*, 2015]. In the SCS, based on 6 years of TOPEX/Poseidon altimeter data, Hwang [2001] noted that the interannual variation of the SCS sea level anomalies is correlated with ENSO. Rong *et al.* [2007] pointed out that the interannual variations of the observed sea level in the SCS are closely related to ENSO through the thermosteric sea level change, especially in the period of 1975–2004, whereas Wu [2013] believed that PDO, instead of ENSO, modulates the SSH interannual variations around the WP. Thus, we explore the possible relationships between pressure difference and PDO and ENSO. Applying the EEMD method to the PDO and ENSO indices, we obtain seven IMFs. The combined time series on interannual time scale includes the fourth and fifth IMFs, while the decadal time scale consists of the sixth and seventh IMFs. Figure 8 shows the comparison of pressure difference of the KSTF with PDO index on decadal time scales (top plot) and the pressure difference of the MSTF with ENSO index on interannual time scale (bottom plot). It is clear that the variability of pressure difference of the KSTF and PDO is quite consistent on the decadal time scale. As mentioned above, the part of the pressure difference relative to the KSTF is mainly controlled by SSH in the EIO, while the PDO may regulate the KSTF through the SSH changes in the EIO. The connection between PDO and SSH in the EIO is deferred to future study.

The bottom plot of Figure 8 shows that the pressure difference of the MSTF has a similar variation with ENSO on interannual time scale. The correlation coefficient between ENSO and SSH in region K (A) on the interannual time scale is around -0.88 (-0.05). Consistent with variance analysis, ENSO regulates the MSTF mainly through SSH in the Sulawesi Sea. Gordon *et al.* [2012] pointed out that the MSTF supplies the low-salinity surface layer waters into the western Sulawesi Sea during prolonged El Niño periods. This builds a pool of buoyant surface water that inhibits the surface layer contribution from the western tropical Pacific warm water, via the Mindanao Current, into the Makassar Strait. Therefore, SSH in the Sulawesi Sea may

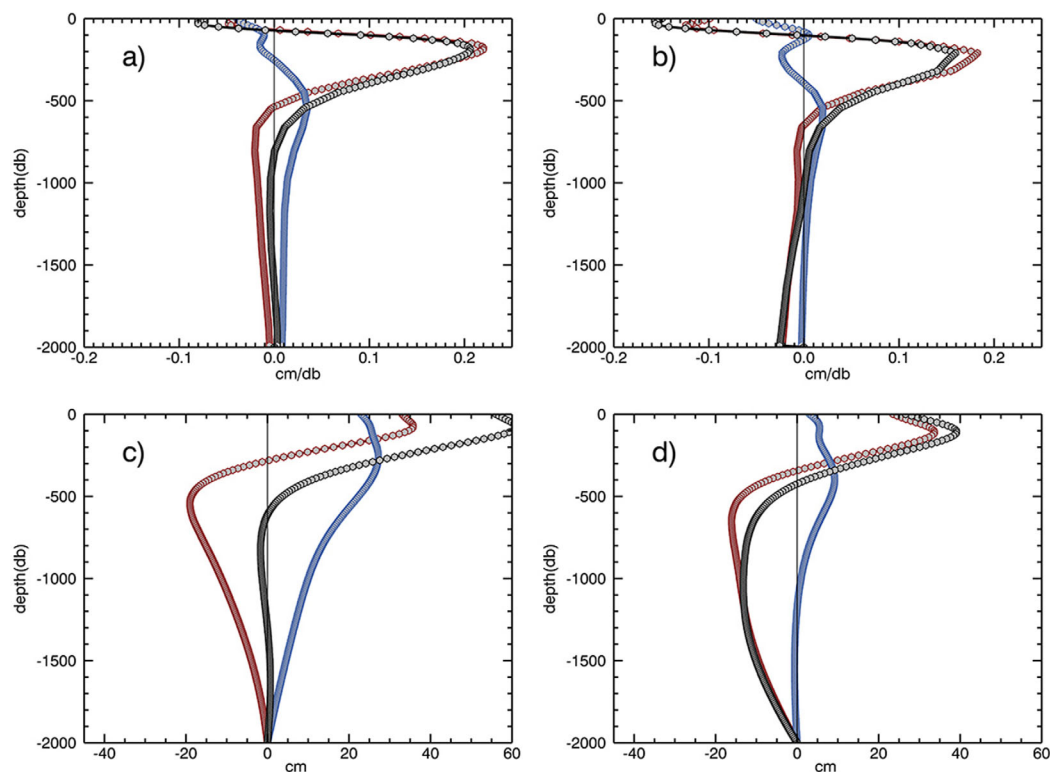


Figure 9. Vertical profiles of the thermal/haline contribution to the dynamic height difference between the beginning and end of the two pathways, averaged over 1958–2007. The thermal contribution term (Red), haline contribution term (Navy), and total dynamic height difference (Black) at each pressure level are shown in (a) for the KSSTF and (b) for the MSTF. The vertically accumulated thermal contribution term (Red) and haline contribution term (Navy) to the dynamic height difference, and total dynamic height (Black) difference, based on a reference pressure of 2000db are shown in (c) for the KSSTF and (d) for the MSTF.

According to equation (2), the dynamic height difference is zero at the reference pressure, and it gradually changes with decline in pressure. We start with the 50 year climatological mean of the dynamic height difference from ORAS4. The top plots of Figure 9 show the vertical profiles of the thermal and haline contributions to the dynamic height difference between the beginning and end of the pathways at each pressure level.

Figure 9a is for the KSSTF. In general, the thermal contribution to the dynamic height difference is mainly confined to the layer above 600 db. Within the top 80 db, the thermal contribution is negative, which may result from a sea surface temperature difference due to the latitudinal difference between region A ($\sim 20^{\circ}\text{N}$) and B ($\sim 10^{\circ}\text{S}$). The thermal contribution is positive in the depth range of 80–600 db, indicating that the water temperature in region A is warmer than region B within this depth range. This is primarily due to the influence of the Kuroshio, the warm western boundary current in the northwestern Pacific. Below the 600 db depth, the thermal contribution becomes negative; this is likely due to the temperature difference of the intermediate water mass in the WP and EIO [Talley *et al.*, 2011].

The haline contribution is negative in the upper 300 db because in this depth range the water in region A is saltier than that in region B. The salinity difference is due to the combined effect of local evaporation minus precipitation and salt/freshwater advection. Below 300 db, the haline contribution is positive because the water in the Indian Ocean is saltier than that in the Pacific [Talley *et al.*, 2011]. Haline and thermal contributions have opposite signs below the 600 db level; in particular, below the 1000 db level they have similar magnitude and thus tend to compensate each other.

Figure 9c shows the cumulative contributions of thermal and haline terms at each level, starting from the 2000 db reference level. It is readily seen that the cumulative temperature contributions become positive above the 300 db depth. It is approximately 32 cm at the surface. The cumulative salinity contribution is always positive. It is around 23 cm at the surface. Therefore, the total dynamic height difference between

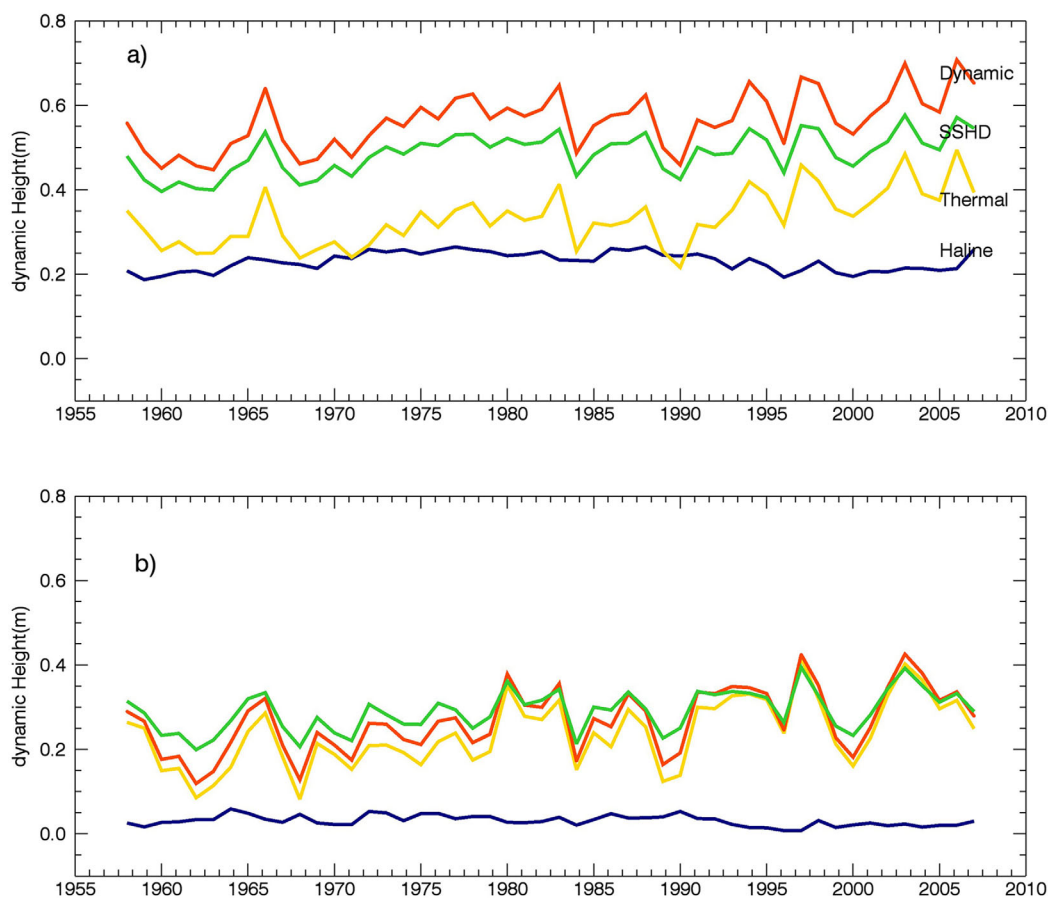


Figure 10. The time evolution of thermal contribution term (Yellow), haline contribution term (Navy), total dynamic height difference (Red), and SSHD (Green); (a) between region A and region B; (b) between region A and region K.

east of the Luzon Strait and south of the Sunda Strait is 55 cm. The thermal contribution to the dynamic height difference is larger than the haline contribution. The total cumulative dynamic height difference is slightly higher than the mean sea surface height difference of 49 cm shown in Figure 2a. This difference is due to the fact that SSH in Figure 2a is directly taken from the sea level data in ORAS4, while the dynamic height difference at sea level shown in Figure 9c is based on the thermal wind relation and the choice of reference pressure of 2000 db.

For the MSTF, Figure 9b shows the profiles of the thermal and haline contributions to the dynamic height difference between regions A and K, averaged over 1958–2007. Similar to the case of the KSSTF, thermal contribution to the dynamic height difference is mostly confined to the upper 600 db. In the first 100 db, the thermal contribution is negative, which may be due to the sea surface temperature difference associated with the latitudinal difference between region A ($\sim 20^\circ\text{N}$) and K ($\sim 4^\circ\text{N}$). The thermal contribution is positive in the depth range of 100–600 db, indicating that the water temperature in region A is warmer than in region K over this depth range. It may also be due to the influence of the Kuroshio. Below 600 db depth, the thermal contribution is negative, which may be due to the fact that the intermediate water in the Sulawesi Sea is warmer than the North Pacific Intermediate Water east of the Luzon Strait [Talley *et al.*, 2011]. The haline contribution is negative above 400 db, indicating that water at this level in region A is saltier than that in region K. Qu *et al.* [1999] have discussed the climatological circulation and water mass distribution near the Philippine Coast. High-salinity east of the Luzon Strait may be linked to the formation of the relatively salty North Pacific Tropical Water (NPTW) due to the excessive evaporation in this region. Gordon *et al.* [2012] have revealed that there is the fresher water originated from SCS by way of the MSTF into the Sulawesi Sea in an El Niño year. Another cause, we postulate, is the intensified precipitation resulted from the Madden Julian Oscillations, which reduces the salinity in the Sulawesi Sea [Rauniyar and Walsh, 2011]. In

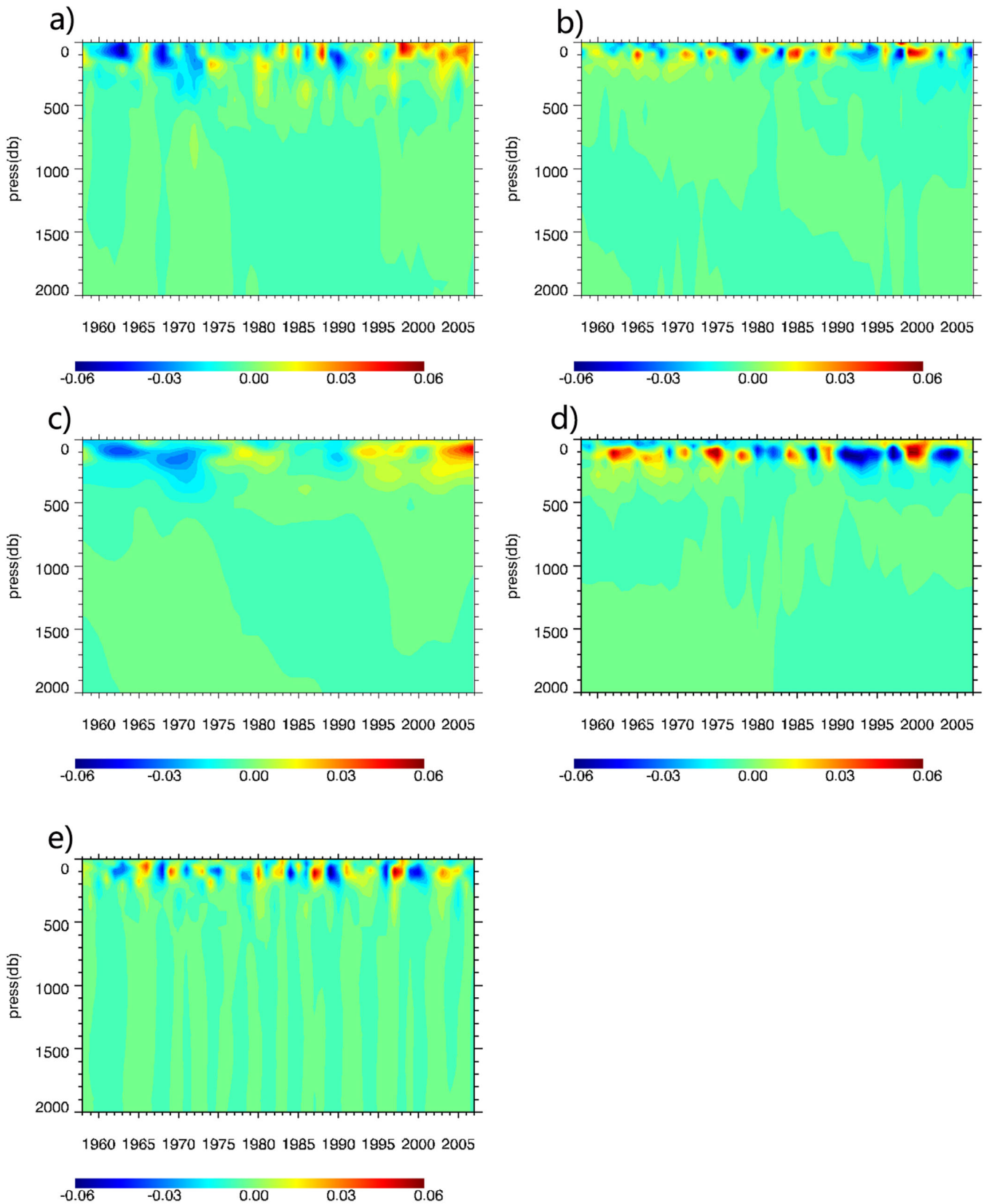


Figure 11. Time evolution of the annual mean anomalous thermal contribution term in each layer: (a) for region A; (b) for region B; (c) is decadal variations of (a) and (b); (d) for region K; ϵ is the interannual variation of (a)–(d); color maps in unit of cm/db. The time series of Figure 11c was obtained by 9-point low-pass filtering to show the decadal variations. The interannual time series ϵ (e) was obtained by 9-point high-pass filtering of (a)–(d).

the layer of 400–1200 db, the haline contribution reverses and becomes positive. Different subsurface water and intermediate water masses in the WP and the Sulawesi Sea may be the main cause [Qu *et al.*, 1999]. Figure 9d shows the cumulative contributions of thermal and haline terms integrated from the 2000 db reference level. The cumulative thermal contributions become positive above 350 db depth. It is about 23 cm at the surface. The cumulative haline contribution is about 3 cm at the surface. Therefore the total dynamic height difference between east of the Luzon Strait and the Sulawesi Sea is 26 cm, which is slightly smaller than the mean sea surface height difference (29 cm) in Figure 2b. The magnitude of haline contribution is ~13% of thermal contribution.

Figures 10a and 10b show the time series of thermal and haline contribution to dynamic height differences (using again the 2000 db as the reference pressure) for the KSSTF and MSTF, respectively. We also plot the sum of the dynamic height differences and sea surface height difference in Figure 10 for comparison. It is clear that the variability of dynamic height difference matches that of the sea surface height difference quite closely; thus, our analysis based on water column (T, S) properties and using the traditional reference level is rather acceptable for the study of variability in this oceanic region. For both the KSSTF and MSTF, the variability of thermal contribution dominates the dynamic height variations. The haline term also provides some minor contribution to the interannual and decadal variations, more so for the KSSTF. This result partially supports the idea that the thermal effect is the main contributor to sea level variations as noted in earlier studies [e.g., Levitus *et al.*, 2000].

Thermal dynamic height variations may be caused by variations in temperature in the subsurface layers. For each region, equation (1) can be rewritten in terms of temperature deviation from its climatological mean

$$\delta h(p_0, p_1) \approx \frac{1}{g\rho_0} \int_{p_0}^{p_1} \alpha(T - \bar{T}) dp - \frac{1}{g\rho_0} \int_{p_0}^{p_1} \beta(S - \bar{S}) dp \quad (3)$$

Figure 11 shows the evolution of the annual mean anomalous thermal height contribution, the first term on the right-hand side of equation (3), in each layer in region A, B, and K. Figures 11a, 11b, and 11c are related to the KSSTF. Here, our focus is on the decadal variation. In region A, the large anomalous thermal term is confined between 0 and 400 db; while in region B, the high value of this term is confined to the upper 300 db. Decadal variability (Figure 11c) can penetrate to the upper 500 db, with the large value mostly confined to the upper 300 db. A transition occurs around 1972: before 1972 the anomalous thermal contribution is mostly negative in region A and positive in region B; from 1973 to 1984, the increase of thermal contribution is primarily due to the positive contribution from region A; from 1985 to 1990, the positive anomalous thermal contribution from region B reduces the net thermal term in the upper ocean; after 1991 both the positive anomalous thermal contribution from region A and negative anomalous from region B further enhance the net thermal term in the upper ocean.

Figures 11a, 11d, and 11e are related to the MSTF. Comparing Figure 11a with Figure 11d, interannual variability in region K has a slightly larger magnitude than that in region A in the upper 400 db. It is consistent with the variance analysis discussed in section 3. There are different situations corresponding to complicated dynamic and thermodynamic contributions in different years. For instance, Figure 11e shows low values in 1962–1963 and 1999–2001, while a similar phenomenon can also be found in Figure 6. However, Figures 11a and 11d indicate that these two cases are due to different mechanisms. In 1962–1963, the thermal effect in region A gives rise to negative anomalies within the upper 200 db, while it is a largely positive anomaly in region K within the 200–300 db level. Therefore, their difference is negative. In 1999–2001, thermal effects in the upper layer (0–200 db) in both regions A and K are very pronounced, and their difference is negative since the thermal term in region A is smaller than in region K.

6. Conclusions

The results of our analysis for pressure differences at the beginning and end of two branches of the SCSTF, (i.e., KSSTF and MSTF) are as follows.

1. For the KSSTF, the pressure difference between the WP and the EIO is closely correlated to the volume transport through the Karimata Strait on the decadal time scale. The variability of the WP-EIO pressure

difference is primarily controlled by the variability of SSH in the EIO, which appears to be modulated by PDO.

For the MSTF, variability of the pressure difference between east of the Luzon Strait and the Sulawesi Sea corresponds well to the variability of outflow through the Mindoro Strait on interannual time scale. The variability of this pressure difference contains strong interannual signals closely linked to ENSO. In light of this relation, the interannual variability of the MSTF can be monitored by means of sea level difference.

- Dynamic height difference, a proxy of SSH/pressure difference, is decomposed into the thermal and haline components for each layer over the depth of 0–2000 db. For the KSSTF, more than half of the dynamic height difference, around 32 cm, is due to the water temperature difference between the corresponding regions, while the remaining dynamic height difference, around 23 cm, is due to the salinity difference. For the MSTF, the dynamic height difference is largely due to the seawater temperature difference. It is partly because both regions A and K are located in the WP and have similar salinity in the bottom layers. The thermal component dominates the dynamic height variability. The haline component has rather small interannual and decadal variations. For both the KSSTF and MSTF, pressure differences are mostly confined within the top 600 db.

Our results demonstrate that variability of the SCSTF is primarily regulated by the large-scale thermohaline and wind-driven circulation in the Pacific/Indian Oceans. Thus, climate changes induced by variability in the WDC and THC in both the Western Pacific and eastern Indian Oceans can affect the SCSTF. Further study along this line will help us to better understand the regulation of this important component of global circulation.

Appendix A: Regulation of South China Sea Throughflow by Pressure Difference in SODA

As a further support to our conclusion on the SCSTF variability, we show here the consistent result from applying the same approach to SODA products. As introduced in section 2, the horizontal resolution of SODA is $0.5^\circ \times 0.5^\circ$, finer than ORAS4. Similar to Figure 1, Figure A1 shows the western branch of the SCSTF, termed as the Karimata Strait Throughflow (KSTF) in distinguishing from the KSSTF in ORAS4. The KSTF consists of the Kuroshio water entering the northern SCS via the Luzon Strait, exiting from the Karimata Strait, and finally feeding into the EIO via the Lombok Strait. Such a flow pattern, consistent with *in situ*

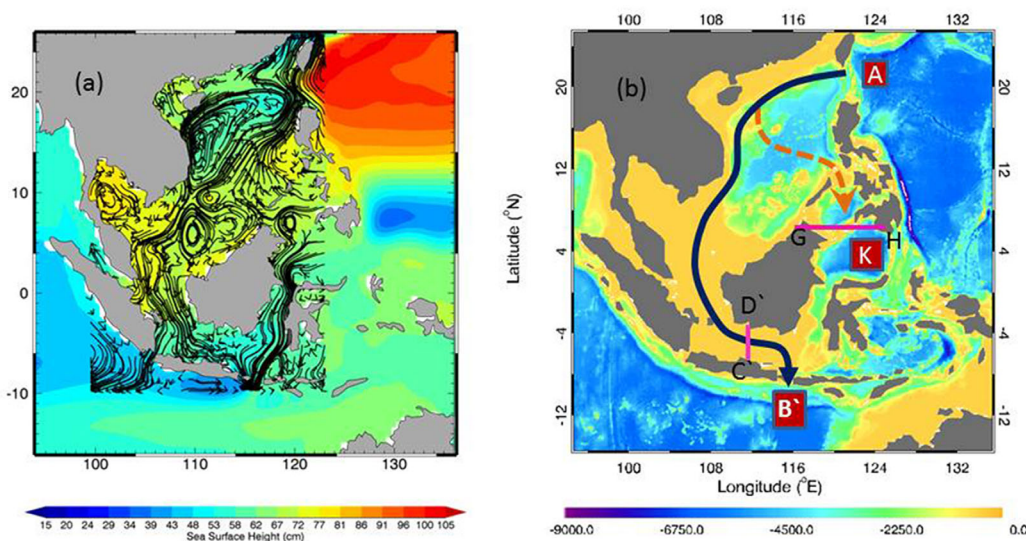


Figure A1. Similar to Figure 1 but using SODA data. (a) 50 year (1958–2007) mean SSH and streamline of ocean current in the upper 50 m layer of the SCS. (b) Topography of the SCS and the schematic drawing of two branches of SCSTF, which are generated from streamlines shown in Figure A1a. For the KSTF, Kuroshio water enters the northern SCS via the Luzon Strait and exits from Karimata Strait, majority of which feeds into the EIO via the Lombok Strait. For the MSTF branch, water exits from the Mindoro Strait to feed into the Sulawesi Sea. The MSTF is problematic in SODA because the flow comes from the western Pacific via the Philippines but not from the South China Sea via the Mindoro Strait as suggested by the upper layer streamlines seen in Figure A1a. Region A is the area of (18.5–21.5°N, 123.5–125.5°E) while Region B' indicates the area of (10.25–12.25°S, 114.25–116.25°E). Region K represents the area of (2.5–4.5°N, 121.5–124.5°E). C' D' and GH indicate the sections at (2.25–6.75°S, 112°E) and (6.5°N, 117.5–124.5°E), respectively.

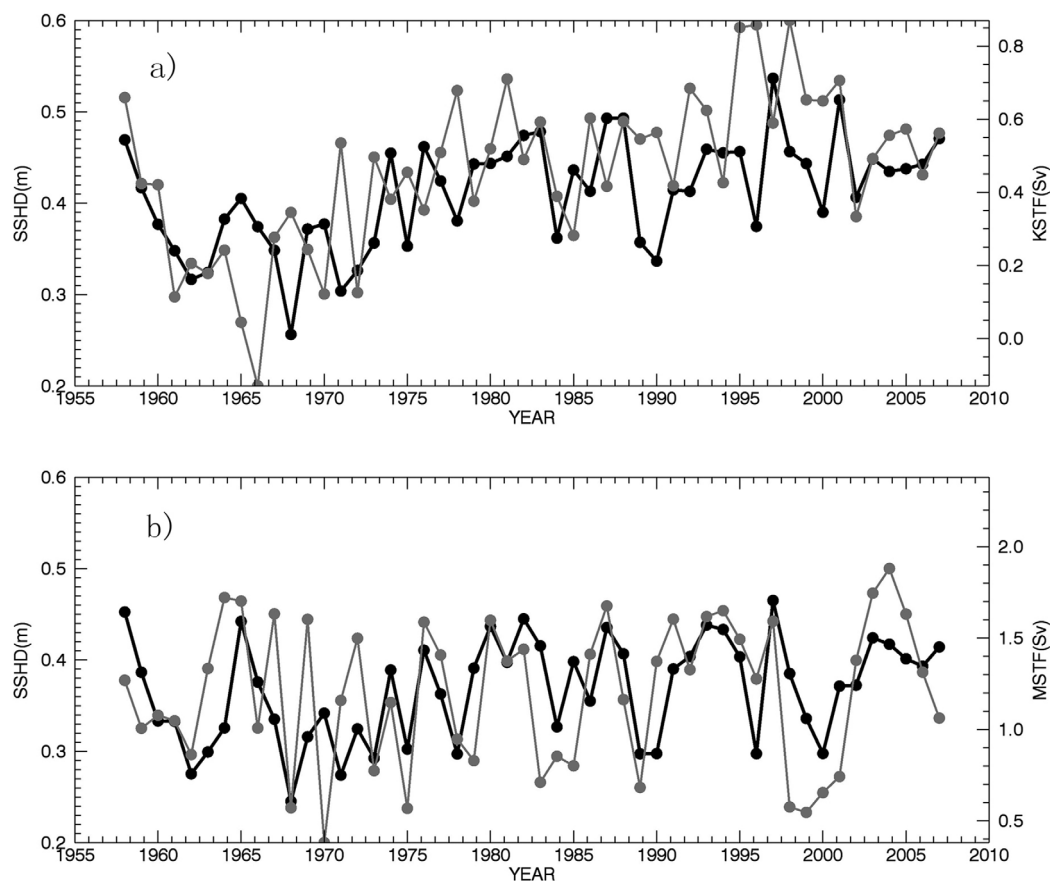


Figure A2. Similar to Figure 2 but for SODA data, (a) the annual mean time series of SSH difference between region A' and B' (black) and volume transport (gray) through section C'D'; (b) SSH difference between region A and K (black) and volume transport (gray) through section GH.

observations of Fang *et al.* [2005], Susanto *et al.* [2013], and Gordon *et al.* [2010], is accompanied by an approximately 41 cm mean SSH difference between east of the Luzon Strait (region A) and south of the Lombok Strait (region B').

Similarly, time series of SSH difference between station A and B' can be used as an index for monitoring the modulation of the pressure-head between the WP and the EIO. Moreover, the transport of KSTF is calculated by vertically and meridionally integrating the zonal flow passing through the C' D' section (2.25–6.25°S, 112°E). Figure A2a shows time series similar to Figure 2a; there are consistent and significant decadal variations that decreased before 1965–1970 and increased afterward. After applying the EEMD, compositions of the sixth, seventh IMFs, and trend component of KSTF volume transport and pressure head are shown in Figure A3a, these are similar to Figure 4. Both the pressure difference and volume transport increased from the late 1960s to late 1970 and from 1992 to 1997, and they decreased from 1980 to 1986 and from 1998 to 2005. Thus, from either ORAS4 or SODA we can draw the conclusion that on decadal timescale the western branch of SCSTF is regulated by the pressure difference between the WP and the EIO.

On the other hand, the upper layer flows in the Sulu Sea are mostly northward, opposite to the conventional notion of the MSTF as indicated by the red dashed line in Figure A1b. This is the reason for us to select ORAS4 as the primary data set in the main body of this study. The calculated MSTF transport from SODA (black line in Figure A2b) is, however, southward with a 50 year mean of ~ 1.2 Sv, implying reversed flows at depth in the Sulu Sea (not shown). Despite of smaller magnitude of variability and long-term trend compared to its counterpart from ORAS4 (see Figure A2b and 2b), the MSTF transport from both data sets shows consistent interannual variations. Moreover, compositions of the third, fourth, and fifth IMFs of MSTF volume transport and pressure head (Figure A3b) are similar to their counterparts from ORAS4 (see Figure 6).

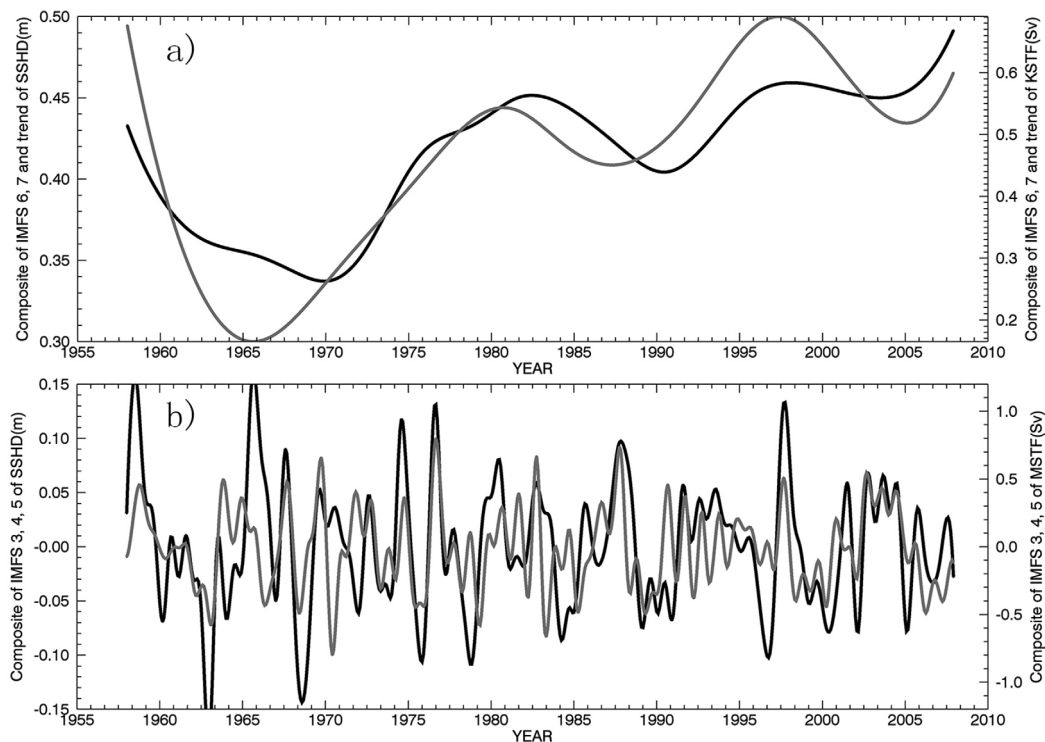


Figure A3. (a) Similar to Figure 4 but for SODA data. Time series of the combination of the sixth, seventh intrinsic mode functions and trend function of the EEMD components of pressure head (black) and volume transport (gray) in Figure A2; (b) Similar to Figure 6 but for SODA data, the combined time series (consisting of the third, fourth, and fifth intrinsic mode functions of EEMD components) of pressure head (black) and volume transport (gray).

Acknowledgments

Both ORAS4 and SODA are available on the server of the Asia-Pacific Data Research Center (APDRC) of the International Pacific Research Centre (IPRC). The ORAS4 outputs were downloaded from http://apdrc.soest.hawaii.edu/datadoc/ecmwf_oras4.php, and SODA 2.0.2 and 2.0.4 were downloaded from <http://apdrc.soest.hawaii.edu/las/v6/dataset?catitem=3017>. The EEMD code is provided by Research Center for Adaptive Data Analysis, Taiwan (<http://rcada.ncu.edu.tw/research1.htm>). This work was supported by the Strategic Priority Research Program of the Chinese Academy of Sciences (grant XDA11010304), the National Natural Science Foundation of China (grant number 41306015 and 41476013) and the Independent Research Project Program of State Key Laboratory of Tropical Oceanography (grant LTOZZ1603). Constructive comments from two anonymous reviewers and Editor Dr. Lie-Yauw Oey helped us greatly improve the presentation of this study.

References

Aagaard, K., A. T. Roach, and J. D. Schumacher (1985), On the wind-driven variability of the flow through Bering Strait, *J. Geophys. Res.*, *90*(C4), 7213–7221, doi:10.1029/JC090iC04p07213.

Balmaseda, M. A., K. Mogensen, and A. T. Weaver (2013), Evaluation of the ECMWF Ocean Reanalysis ORAS4, *Q. J. R. Meteorol. Soc.*, *139*, 1132–1161, doi:10.1002/qj.2063.

Carton, J. A., and B. S. Giese (2008), A reanalysis of ocean climate using simple ocean data assimilation (SODA), *Mon. Weather Rev.*, *136*, 2999–3017.

Castruccio, F. S., E. N. Curchitser, and J. A. Kleypas (2013), A model for quantifying oceanic transport and mesoscale variability in the Coral Triangle of the Indonesian/Philippines Archipelago, *J. Geophys. Res. Oceans*, *118*, 6123–6144, doi:10.1002/2013JC009196.

Cazenave, A., and W. Lovel (2010), Contemporary sea level rise, *Annu. Rev. Mar. Sci.*, *2*, 145–173.

D’Addezio, J. M., B. Subrahmanyam, E. S. Nyadjro, and V. S. N. Murty (2015), Seasonal Variability of Salinity and Salt Transport in the Northern Indian Ocean, *J. Phys. Oceanogr.*, *45*(7), 1947–1966, doi:10.1175/JPO-D-14-0210.1.

Fang, G., D. Susanto, I. Soesilo, Q. Zheng, F. Qiao, and Z. Wei (2005), A note on the South China Sea shallow interocean circulation, *Adv. Atmos. Sci.*, *22*, 945–954.

Frankcombe, L. M., S. McGregor, and M. H. England (2015), Robustness of the modes of Indo-Pacific sea level variability[J], *Clim. Dyn.*, *45*(5), 1281–1298, doi:10.1007/s00382-014-2377-0.

Franzke, C. (2012), Nonlinear trends, long-range dependence, and climate noise properties of surface temperature, *J. Clim.*, *25*, 4172–4183.

Gordon, A. L., and R. A. Fine (1996), Pathways of water between the Pacific and Indian oceans in the Indonesian seas, *Nature*, *379*, 146–149.

Gordon, A. L., R. D. Susanto, and A. L. Ffield (1999), Throughflow within Makassar Strait, *Geophys. Res. Lett.*, *26*(21), 3325–3328, doi:10.1029/1999GL002340.

Gordon, A. L., J. Sprintall, H. M. Van Aken, R. D. Susanto, S. Wijffels, R. Molcard, A. Ffield, W. Pranowo, and S. Wirasantosa (2010), The Indonesian throughflow during 2004–2006 as observed by the INSTANT program, *Dyn. Atmos. Oceans*, *50*, 115–128, doi:10.1016/j.dynatmoce.2009.12.002.

Gordon, A. L., B. A. Huber, E. J. Metzger, R. D. Susanto, H. E. Hurlburt, and T. R. Adi (2012), South China Sea throughflow impact on the Indonesian throughflow, *Geophys. Res. Lett.*, *39*, L11602, doi:10.1029/2012GL052021.

Han, W., J. Vialard, M. J. McPhaden, T. Lee, Y. Masumoto, M. Feng, and W. Ruijter (2014), Indian Ocean decadal variability: A review. *Bull. Am. Meteorol. Soc.*, *95*, 1679–1703, doi:10.1175/BAMS-D-13-00028.1.

Huang, M., L. Wu, S. R. Long, S. S. Shen, W. D. Qu, P. Gloersen, and K. L. Fan (1998), The empirical mode decomposition and the Hilbert spectrum for nonlinear and non-stationary time series analysis. *Proc. R. Soc. London Ser. A*, *454*, 903–993.

Hwang, C. (2001) Interannual variation of sea level of South China Sea and its relationship with ENSO, paper Presented at the ASPG Fourth Workshop, ASPG Manage. Board and the Shanghai Astron. Obs., CAS, Shanghai, P.R. China, 14–19 May.

Köhl, A., (2014), Detecting Processes contributing to interannual halosteric and thermosteric sea level variability, *J. Clim.*, *27*, 2417–2426, doi:10.1175/JCLI-D-13-00412.1.

Krishnan, R., and M. Sugi (2003), Pacific decadal oscillation and variability of the Indian summer monsoon rainfall, *Clim. Dyn.*, *21*, 233–242.

- Levitus, S., J. I. Antonov, T. P. Boyer, and C. Stephens (2000), Warming of the world ocean, *Science*, 287(5461), 2225–2229.
- Liu, Q., D. Wang, and Q. Xie (2012), The South China Sea throughflow: Linkage with local monsoon system and impact on upper thermal structure of the ocean, *Chin. J. Oceanol. Limnol.*, 30, 1001–1009.
- Mantua, N. J., S. R. Hare, Y. Zhang, J. M. Wallace, and R. C. Francis (1997), A Pacific interdecadal climate oscillation with impacts on salmon production, *Bull. Am. Meteorol. Soc.*, 78, 1069–1079.
- Morimoto, A., and T. Yanagi (2001), Variability of sea surface circulation in the Japan Sea, *J. Oceanogr.*, 57(1), 1–13.
- Nan, F., H. Xue, F. Chai, D. Wang, F. Yu, M. Shi, P. Guo, and P. Xiu, (2013) Weakening of the Kuroshio intrusion into the South China Sea over the past two decades, *J. Clim.*, 26, 8097–8110, doi:10.1175/JCLI-D-12-00315.
- Overland, J. E., and A. T. Roach (1987), Northward flow in the Bering and Chukchi Seas, *J. Geophys. Res.*, 92(C7), 7097–7105, doi:10.1029/JC092iC07p07097.
- Palacz, A., H. Xue, C. Armbrecht, C. Zhang, and F. Chai (2011), Seasonal and inter-annual changes in the surface chlorophyll of the South China Sea, *J. Geophys. Res.*, 116, C09015, doi:10.1029/2011JC007064.
- Qian, C., C. Fu, and Z. Wu (2011), Changes in the amplitude of the temperature annual cycle in China and their implication for climate change research, *J. Clim.*, 24, 5292–5302.
- Qu, T., and Y. T. Song (2009), Mindoro Strait and Sibutu Passage transports estimated from satellite data, *Geophys. Res. Lett.*, 36, L09601, doi:10.1029/2009GL037314.
- Qu, T., H. Mitsudera, and T. Yamagata (1999), A climatology of the circulation and water mass distribution near the Philippine coast, *J. Phys. Oceanogr.*, 29, 1488–1505, doi:10.1175/1520-0485(1999)029<1488:ACOTCA>2.0.CO;2.
- Qu, T., Y.-Y. Kim, M. Yaremchuk, T. Tozuka, A. Ishida, and T. Yamagata (2004), Can Luzon strait transport play a role in conveying the impact of ENSO to the South China Sea?, *J. Clim.*, 17(18), 3643–3656.
- Qu, T., Y. Du, G. Meyers, A. Ishida, and D. Wang (2005), Connecting the tropical Pacific with Indian Ocean through South China Sea, *Geophys. Res. Lett.*, 32, L24609, doi:10.1029/2005GL024698.
- Qu, T., Y. Du, and H. Sasaki (2006), South China Sea throughflow: A heat and freshwater conveyor, *Geophys. Res. Lett.*, 33, L23617, doi:10.1029/2006GL028350.
- Rauniar, S. P., and K. J. E. Walsh (2011), Scale interaction of the diurnal cycle of rainfall over the maritime continent and Australia: Influence of the MJO, *J. Clim.*, 24, 325–348, doi:10.1175/2010JCLI3673.1.
- Roach, A. T., K. Aagaard, C. H. Pease, S. A. Salo, T. Weingartner, V. Pavlov, and M. Kulakov (1995), Direct measurements of transport and water properties through the Bering Strait, *J. Geophys. Res.*, 100(C9), 18,443–18,457, doi:10.1029/95JC01673.
- Rong, Z., Y. Liu, H. Zong, and Y. Cheng (2007), Interannual sea level variability in the South China Sea and its response to ENSO, *Global Planet. Change*, 55(4), 257–272.
- Susanto, R. D., Z. Wei, R. Adi, T. B. Fan, S. Li, and G. Fang (2013), Observations of the Karimata Strait throughflow from December 2007 to November 2008, *Acta Oceanol. Sin.*, 32(5), 1–6, doi:10.1007/s13131-013-0307-3.
- Takikawa, T., and J. H. Yoon (2005), Volume transport through the Tsushima Straits estimated from sea level difference, *J. Oceanogr.*, 61(4), 699–708.
- Talley L. D., G. L. Pickard, W. J. Emery, and J. H. Swift (2011), *Descriptive Physical Oceanography: An Introduction*, 6th ed., 560 pp., Elsevier, Boston.
- Tillinger, D., and A. L. Gordon (2009), Fifty years of the Indonesian Throughflow, *J. Clim.*, 22(23), 6342–6355.
- Wang, D., Q. Liu, R. X. Huang, Y. Du, and T. Qu (2006), Interannual variability of the South China Sea throughflow inferred from wind data and an ocean data assimilation product, *J. Geophys. Res.*, 33, L14605, doi:10.1029/2006GL026316.
- Wu, C. R. (2013), Interannual modulation of the Pacific Decadal Oscillation (PDO) on the low-latitude western North Pacific, *Prog. Oceanogr.*, 110, 49–58.
- Wu, Z., and N. E. Huang (2009), Ensemble empirical mode decomposition: A noise-assisted data analysis method, *Adv. Adapt. Data Anal.*, 1, 1–41.
- Wyrtki, K. (1961), Physical oceanography of the Southeast Asian waters, *NAGA Rep. 2*, 195 pp., Univ. of Calif., The University of California, Scripps Institution of Oceanography. [Available at <http://escholarship.org/uc/item/49n9x3t4>.]
- Wyrtki, K. (1987), Indonesian through flow and the associated pressure gradient, *J. Geophys. Res.*, 92(C12), 12,941–12,946, doi:10.1029/JC092iC12p12941.
- Xu, F.-H., and L.-Y. Oey (2014), State analysis using the Local Ensemble Transporm Kalman Filter (LETKF) and the tree-layer circulation structure of the Luzon Strait and the South China Sea, *Ocean Dyn.*, 64, 905–923.
- Xue, H., F. Chai, N. Pettigrew, D. Xu, M. Shi, and J. Xu (2004), Kuroshio intrusion and the circulation in the South China Sea, *J. Geophys. Res.*, 109, C02017, doi:10.1029/2002JC001724.
- Yaremchuk, M., J. McCreary, Z. Yu, and R. Furue (2009), The South China Sea throughflow retrieved from climatological data, *J. Phys. Oceanogr.*, 39, 753–767, doi:10.1175/2008JPO3955.1.
- Yu, K., and T. Qu (2013), Imprint of the pacific decadal oscillation on the South China Sea throughflow variability, *J. Clim.*, 26(24), 9797–9805.
- Yu, Z., S. Shen, J. P. McCreary, M. Yaremchuk, and R. Furue (2007), South China Sea throughflow as evidenced by satellite images and numerical experiments, *Geophys. Res. Lett.*, 34, L01601, doi:10.1029/2006GL028103.
- Yuan, Y, G. Liao, and C. Yang (2008), The Kuroshio near the Luzon Strait and circulation in the northern South China Sea during August and September 1994, *J. Oceanogr.*, 64, 777–788.
- Yuan, Y, G. Liao, and C. Yang (2009), A diagnostic calculation of the circulation in the upper and middle layers of the Luzon Strait and the northern South China Sea during March 1992, *Dyn. Atmos. Oceans*, 47, 86–113.
- Zhang, X., and J. A. Church (2012), Sea level trends, interannual and decadal variability in the Pacific Ocean, *Geophys. Res. Lett.*, 39, L21701, doi:10.1029/2012GL053240.